Chaos, Solitons and Fractals 145 (2021) 110787

Contents lists available at ScienceDirect

Chaos, Solitons and Fractals

Nonlinear Science, and Nonequilibrium and Complex Phenomena

journal homepage: www.elsevier.com/locate/chaos

Coulostatics in bioelectrochemistry: A physical interpretation of the electrode-tissue processes from the theory of fractional calculus

E. Hernández-Balaguera

Escuela Superior de Ciencias Experimentales y Tecnología, Universidad Rey Juan Carlos, C/ Tulipán, s/n, 28933 Móstoles, Madrid, Spain

ARTICLE INFO

Article history:
Received 9 July 2020
Revised 23 December 2020
Accepted 13 February 2021

Keywords:
Coulostatic method
Cell membrane
Biological tissue
Fractional calculus
Constant phase element
Biointerface

ABSTRACT

In this paper, we analyze the electrical response of an electrode-tissue-electrode system to the application of a dc current for a sufficiently short time in order to obtain coulostatic conditions: A finite amount of charge is "instantaneously" and efficiently transferred to the capacitors formed by biological membranes at the tissue level and the electrode biointerfacial regions. To allow a more realistic study, the capacitances formed by the electrode-tissue interfaces and those of the cell membranes were modeled using constant phase elements (CPEs). The mathematical expressions for the current, voltage, and charge of the CPEs are obtained in response to the sudden injection of the controlled electric charge. It is predicted theoretically how, under certain conditions, the current path could be restricted to flow through the capacitors formed by the electrode-tissue interfaces and those of the cell membranes, and thus, the total charge injected is practically transferred to both types of capacitance (i.e., a coulostatic charge injection). Finally, we study the influence of the pulse shape (retaining the coulostatic nature) on the technique, from the theoretical perspective of the fractional calculus. The shape of the excitation signal is shown to play a dominant role in the coulostatic relaxation processes, in sharp contrast to the conventional approach. This methodology could be extended to include the membranes of organelles and also to implement a coulostatic test method involving electrical characterizations of biological tissues.

1. Introduction

From the study of electrical circuit theory, we know that an impulse current flowing through a capacitor yields an instantaneous (in zero time) step-charge or, equivalently, a step voltage. This has been used in electrochemistry to quickly charge the double-layer capacitance, so that the faradaic current flowing during the charging process can be neglected [1]. The subsequent impulse response (open-circuit voltage) is a relaxation process which allows the kinetic parameters of the electrode reactions to be determined [1–3]. For instance, an exponential relaxation is obtained in the simplest, most basic case (i.e., an ideal double-layer capacitance in parallel with a polarization resistance) [4]. This procedure is known as the coulostatic test method [1–5].

In bioelectrics, the coulostatic charging process can also be extended to cells or tissues (see below). Specifically, consider two electrodes placed in a portion of tissue, as shown in Fig. 1(a). An electric current $i(t)$ is applied from the electrode on the left and gathered at the electrode on the right. The electrical equivalent circuit (EEC) of Fig. 1(b), consisting of a constant phase element (CPE_{ET}) and a polarization resistance R_P, models the electrode-tissue biointerface [5,6]. Fig. 1(c) shows the EEC of the tissue (see Fig. 1(a)), where the extra- (blue) and intra-cellular (pink) environments are modeled as resistive components (R_E and R_I, respectively), and the cell membranes (green) as a non-ideal capacitive element (CPE_{CM}) [7,8]. As the two EECs shown in Fig. 1(b) and (c) are connected in series, they carry the same input current $i(t)$ and, consequently, the same charge. The biointerface on the right side is not shown in Fig. 1 because its electrical behavior is considered to be identical to that on the left.

Note that CPE_{ET} and CPE_{CM} take into account the space distribution of the electrical properties of the biointerface and the tissue, respectively [5,7,8]. The currents, $i_{Q_{ET}}(t)$ and $i_{Q_{CM}}(t)$, and voltages, $v_{Q_{ET}}(t)$ and $v_{Q_{CM}}(t)$, for both CPEs are indicated in the EECs of Fig. 1(b) and (c). Remember that in a CPE the current $i_Q(t)$ is proportional to the derivative of non-integer order (d^α/dt^α, $0<\alpha<1$) of the voltage $v_Q(t)$ across it [5,7]:

$$i_Q(t) = Q\frac{d^\alpha v_Q(t)}{dt^\alpha} \tag{1}$$

where Q has the units of (farads)×(seconds)$^{\alpha-1}$ with $i_Q(t)$ in amperes, $v_Q(t)$ in volts, and t in seconds. Eq. (1) describes an ideal capacitor (C) for the case $\alpha=1$: $i_C(t)=C(dv_C(t)/dt)$. It can be rewrit-

E-mail address: enrique.hernandez@urjc.es

https://doi.org/10.1016/j.chaos.2021.110787

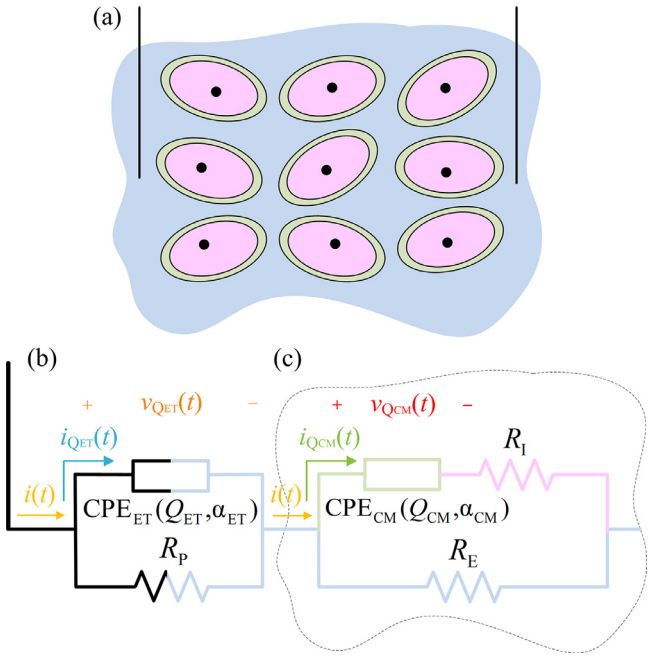

Fig. 1. (a) Illustration of two electrodes placed into a portion of biological tissue which constitutes an electrode-tissue-electrode system. The tissue is represented as a group of similar eukaryotic cells where intra- and extra-cellular spaces, cell membranes and nuclei are shown in pink, blue, green, and black, respectively. Electrical equivalent circuits (EECs) of the system indicated in Fig. 1(a): (b) single electrode-tissue biointerface, where the constant phase element (CPE_{ET}) of parameters Q_{ET} and α_{ET}, and the polarization resistance (R_P), make up the two-element fractional-order model; (c) tissue, where the membrane's capacitive properties are modeled by the CPE_{CM} of parameters Q_{CM} and α_{CM}, and R_I and R_E are the intra- and extra-cellular resistance associated with the electrolytic solutions of each compartment, respectively. (For interpretation of the references to color in this figure legend, the reader is referred to the web version of this article.)

ten in terms of the accumulated charge on the CPE, $q_Q(t)$, as [9]

$$q_Q(t) = Q\frac{\mathrm{d}^{\alpha-1}v_Q(t)}{\mathrm{d}t^{\alpha-1}}$$

where, for convenience, the fractional integral of order $1-\alpha$ ($0<\alpha<1$) is expressed in terms of a fractional derivative of order $\alpha-1$ (negative value). Although it is not the case here, it is important to note that the scientific literature has shown that the capacitive response of a number of real-world systems, such as batteries [10–12], supercapacitors [12,13], and/or photo-electrochemical cells [14–16], also exhibits non-ideal dynamics, which leads directly to fractional-order phenomena or, more specifically, CPE effects. This complicated behavior, which manifests itself mathematically as Cole-Cole relaxation processes or power-law decays, reveals the fractional-order nature of anomalous (history-dependent) events occurring in a wide range of applications in many branches of science and engineering [17]. In effect, besides providing simplicity and goodness-of-fit with experimental data, the ubiquitous fractional-order capacitors (CPEs) predict the capacitive features of complex systems, providing an explanation of the underlying mechanisms.

Now, for the moment, let the CPEs of Fig. 1(b) and (c) be ideal capacitors (C_{ET} and C_{CM}), initially discharged, and $i(t)$ an impulse source, that is,

$$i(t) = q_{in}\delta(t) \tag{2}$$

where $\delta(t)$ is the unit-impulse (or Dirac delta) function and q_{in} is the charge associated with the impulse (strength of the impulse). Theoretically speaking, q_{in} is transferred in zero time to each of the EECs of Fig. 1(b) and (c):

$$i(t) = 0, \quad t \neq 0$$

$$\int_{-\infty}^{\infty} i(t)\ \mathrm{d}t = q_{in}$$

A quick analysis can be done as follows. While the current impulse is applied ("zero" duration), the electrical inertia exhibited by both EECs, due to the capacitive components, allows us to replace the capacitors with short circuits (zero initial voltages). Note that R_P is short-circuited by C_{ET} and ideally non-faradaic current flows. Just after applying the impulse, the amounts of charge of q_{in} and $q_{in}R_E/(R_E+R_I)$ are transferred instantaneously to C_{ET} and C_{CM}, respectively. In the latter case, the charge q_{in} transferred is reduced by the factor $R_E/(R_E+R_I)$ and, thus, the coulostatic charging process in a tissue is limited by the extracellular path R_E. We note that if $R_E \gg R_I$ [18], practically all the current is forced to flow through the cell membranes, which favors the interaction between the current injected and the cell membranes. Therefore, an efficient approach for coulostatic charging of the electrode-tissue-electrode system enables "abruptly" (compared to its "electrical inertia") transferring almost all the charge injected into the system to the capacitors formed by the electrode-tissue interfaces and those of the cell membranes. In other words, almost all the charging current flows through them.

Nevertheless, in the context of the coulostatic method, the dynamic behavior of the electrode-tissue-electrode system is significantly complicated by the presence of CPEs. The fractional-order capacitors give rise to a meaningful acceleration of the initial regime of the responses during the coulostatic charge injection. The transition from the discharge state to the specific instant at which the total charge (q_{in}) has been transferred to the CPEs is described in terms of asymptotic power laws –a characteristic pattern of fractional relaxation processes–. Consequently, a decrease in the value of α results in faster responses, leading from linear relations ($\alpha=1$: exponential mode relaxation) to non-linear patterns ($0<\alpha<1$: fractional dynamics approach). Furthermore, it should be emphasized that the fractional-order α also alters the dynamics of the current, voltage, and charge of the CPEs at multiple time scales (timescale-dependent processes). Special functions emerge when dealing with differential equations of non-integer order, implying that the coulostatic relaxation curves are not described in terms of the same functions. In effect, the voltage and current (charge) of the CPEs are related by a fractional derivative (integral). Note that classical exponential processes represent timescale invariant phenomena. Thus, if one imposes the following conditions: (i) all the charge injected q_{in} is transferred to the CPEs; (ii) the step-charge changes the voltage across the fractional-order capacitors by a value inversely proportional to the "pseudo-capacitances" (i.e., almost all the current flows through the CPEs); different constraints are obtained, in sharp contrast to the conventional approach. The most restrictive condition should therefore be selected, taking into account the electrical inertia of the interfaces and the tissue.

From the discussion above, two valuable effects can be expected during a coulostatic charge injection: (i) The faradaic reactions can be neglected [1,4], that is, no electrons are transferred between the electrode and the tissue, and thus, damage to the tissue (by heating, pH changes or accumulation of toxic electrochemical products changes [6,19]) or to the electrode itself is minimized; and (ii) electric field interactions with the cell membrane (or even intracellular structures) are favored. Specifically, although it is not the case here, sufficiently short-pulsed electric fields (respect to the cell and organelle membrane charging times) are capable of inducing effects on subcellular organelles (such as nuclei and mitochondria), which is of interest in bioengineering and for biomedical applications [20,21].

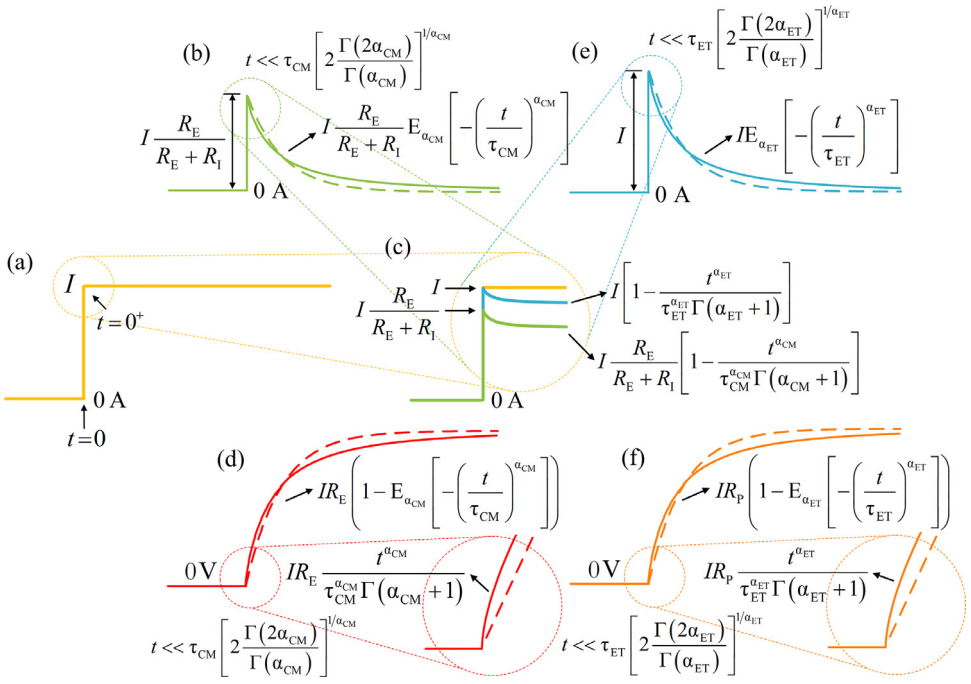

Fig. 2. Waveforms during the charge injection: (a) applied step current $i(t)$, of height I, in the electrode-tissue-electrode system; (b) resulting current and (d) voltage CPE_{CM} responses, $i_{Q_{CM}}(t)$ and $v_{Q_{CM}}(t)$, respectively; (e) current and (f) voltage step responses of the CPE_{ET}, $i_{Q_{ET}}(t)$ and $v_{Q_{ET}}(t)$, respectively. Insets in Fig. 2(d) and (f) show expanded views of the transient-voltage responses at sufficiently short times. Fig. 2(c) shows the applied step current of height I at sufficiently short times, together with the waveforms of the resulting currents of CPE_{CM} and CPE_{ET}. Dashed and solid lines indicate the step responses by considering $\alpha=1$ (exponential behavior) and $0<\alpha<1$ (non-exponential dynamic), respectively. (For interpretation of the references to color in this figure legend, the reader is referred to the web version of this article.)

The practical implementation of the coulostatic method requires the use of fractional calculus [5,22,23] by including the non-ideal capacitances CPEs, and to approximate the effect of an impulse current ("infinite" height and "zero" duration). The latter can be achieved by a rectangular current pulse whose width is sufficiently short compared to the time constants of the electrode-tissue-electrode system under study [5]. In the context of literature, modified versions of the charge-step method, based on the use of finite (or "non-zero") pulse durations, have been described, motivated by the experimental limitations of the technique [24]. In effect, the shape of the pulse (e.g., rectangular, triangular or delta function) is unimportant as long as the coulostatic nature is maintained and ideal capacitors are considered [1,25]. However, this idea cannot be extrapolated by considering CPEs. The theory of fractional calculus emerges in order to accurately analyze the non-ideal capacitive response of an electrode-tissue-electrode system, introducing a multiscale generalization inherent in the definition of the non-integer order derivative over a wide range of space and time. Special functions describe tissue and biointerface complexity through parameters that arise from fractional operators within the underlying differential equations of non-integer order. In turn, it makes analysis of the charge injection processes (width of the pulse required to guarantee an efficient coulostatic approach) and the subsequent relaxation phenomena (importance of the pulse shape) more difficult. These are several reasons why further progress on the knowledge of the coulostatic method is indeed necessary.

The aim of this paper is to establish the required conditions for a coulostatic charge injection into the electrode-tissue-electrode system shown in Fig. 1(a) while a dc current is applied, as well as the study of the subsequent relaxation processes using the mathematical tools of fractional calculus. We firstly obtain mathematical expressions for the current, voltage, and charge for each of the CPEs shown in Fig. 1(b) and (c), in response to a current-step input of height I (see Fig. 2(a)). From the above, we then obtain the constraints on the time interval, immediately after the current is applied, during which an efficient coulostatic charge injection occurs. Lastly, a detailed analysis of the impact of the pulse shape on the coulostatic technique (focused mainly on the timescale just after the current interruption) is carried out to shed light on the essential differences between the conventional and generalized procedure. The methodology described in this paper can be extended to consider the organelle membranes of intracellular structures.

2. Theoretical background

From LTI (linear time-invariant) circuit theory, we know that the natural response of a first-order circuit involves the exponential function. However, here we will use the Mittag-Leffler function to consider the dynamics imposed by the fractional-order ($0<\alpha<1$) capacitance, CPE (see Eq. (1)). It can be verified that the following fractional ordinary differential equation models the voltage or current $x(t)$ dynamics of the CPEs when the EECs of Fig. 1(b) and (c) are driven by a step current source, $i(t)=Iu(t)$ ($u(t)$ is the standard Heaviside function),

$$\frac{\mathrm{d}^{\alpha}x(t)}{\mathrm{d}t^{\alpha}}+\frac{x(t)}{\tau^{\alpha}}=\frac{x(\infty)}{\tau^{\alpha}} \tag{3}$$

where $x(\infty)$ is the steady-state value. In effect, the forced response, found at $t\to\infty$, can be obtained from the knowledge of dc circuits (constant value), i.e., CPEs act as open circuits (dc steady-state). As shown in [22], Eq. (3) can be solved via the Laplace transformation of the fractional derivative in Caputo sense with $0<\alpha<1$,

$$\frac{\mathrm{d}^{\alpha}}{\mathrm{d}t^{\alpha}}x(t)=\frac{1}{\Gamma(1-\alpha)}\int_0^t\frac{\mathrm{d}x(\tau)}{\mathrm{d}\tau}\frac{\mathrm{d}\tau}{(t-\tau)^{\alpha}}$$

with an analytical solution given by

$$x(t)=x(\infty)+\left(x\left(0^{+}\right)-x(\infty)\right)\mathrm{E}_{\alpha}\left[-\left(\frac{t}{\tau}\right)^{\alpha}\right] \tag{4}$$

where $x(0^+)$ denotes the value of $x(t)$ immediately following the step change. $E_\alpha[-(t/\tau)^\alpha]$ is the one-parameter Mittag-Leffler function, defined as [5,7,22,23]

$$E_\alpha\left[-\left(\frac{t}{\tau}\right)^\alpha\right]=\sum_{k=0}^{\infty}\frac{\left[-\left(\frac{t}{\tau}\right)^\alpha\right]^k}{\Gamma(\alpha k+1)},\quad \alpha>0 \tag{5}$$

where Γ is the Gamma function and τ is the time constant of the EEC under study. For convenience, we also introduce [5,22,23] the two-parameter Mittag-Leffler function $E_{\alpha,\beta}[-(t/\tau)^\alpha]$,

$$E_{\alpha,\beta}\left[-\left(\frac{t}{\tau}\right)^\alpha\right]=\sum_{k=0}^{\infty}\frac{\left[-\left(\frac{t}{\tau}\right)^\alpha\right]^k}{\Gamma(\alpha k+\beta)},\quad \alpha,\beta>0 \tag{6}$$

Note that $E_1[-(t/\tau)^1]=E_{1,1}[-(t/\tau)^1]=e^{-t/\tau}$. The Laplace transform formulas for the fractional derivative and the Mittag-Leffler function are given by

$$\mathcal{L}\left\{\frac{d^\alpha}{dt^\alpha}x(t)\right\}=s^\alpha X(s)-s^{\alpha-1}x(0)$$

$$\mathcal{L}\left\{t^{\beta-1}E_{\alpha,\beta}\left[-\left(\frac{t}{\tau}\right)^\alpha\right]\right\}=\frac{s^{\alpha-\beta}}{s^\alpha+1/\tau^\alpha}$$

We first analyze the EEC shown in Fig. 1(c).

2.1. Current step response of the biological tissue

Let us consider the CPE_{CM} initially discharged. At the instant t=0, a dc current I is applied to the EEC (refer to Fig. 2(a)). Immediately after the step change (i.e., $t=0^+$), CPE_{CM} behaves as a short circuit (CPE voltage cannot change abruptly) and thus, $v_{Q_{CM}}(0^+)=0$ V and $i_{Q_{CM}}(0^+)=IR_E/(R_E+R_I)$. For a sufficiently long-time ($t\to\infty$), all the current flows through R_E: CPE_M blocks the dc current $i_{Q_{CM}}(\infty)=0$ A and is charged to the voltage $v_{Q_{CM}}(\infty)=IR_E$.

Using Eq. (4) with the values found previously, we obtain

$$i_{Q_{CM}}(t)=I\frac{R_E}{R_E+R_I}E_{\alpha_{CM}}\left[-\left(\frac{t}{\tau_{CM}}\right)^{\alpha_{CM}}\right],\quad t>0 \tag{7}$$

$$v_{Q_{CM}}(t)=IR_E\left(1-E_{\alpha_{CM}}\left[-\left(\frac{t}{\tau_{CM}}\right)^{\alpha_{CM}}\right]\right),\quad t>0 \tag{8}$$

where τ_{CM} is the time constant for the EEC of Fig. 1(c):

$$\tau_{CM}=[(R_E+R_I)Q_{CM}]^{1/\alpha_{CM}} \tag{9}$$

where Q_{CM} and α_{CM} are the CPE_{CM} parameters. Note that τ_{CM} can be determined by inspection of the EEC: the current source I is replaced by an open circuit and the CPE_{CM} "sees" the resistance R_E+R_I. Thus, τ_{CM} is the product $(R_E+R_I)\times Q_{CM}$ raised to the $1/\alpha_{CM}$ (to give units of time).

The time-integral of the current $i_{Q_{CM}}(t)$ yields the charge accumulated on CPE_{CM},

$$q_{Q_{CM}}(t)=I\frac{R_E}{R_E+R_I}tE_{\alpha_{CM},2}\left[-\left(\frac{t}{\tau_{CM}}\right)^{\alpha_{CM}}\right],\quad t>0 \tag{10}$$

Now, we rewrite the above expressions at sufficiently short times. Eqs. (5) and (6) can be truncated at the third and second terms, respectively, if $[(t/\tau)^\alpha/\Gamma(\alpha+1)]\gg[(t/\tau)^{2\alpha}/\Gamma(2\alpha+1)]$ and $1/\Gamma(\beta)\gg[(t/\tau)^\alpha/\Gamma(\alpha+\beta)]$, respectively. This gives

$$i_{Q_{CM}}(t)=I\frac{R_E}{R_E+R_I}\left[1-\frac{t^{\alpha_{CM}}}{\tau_{CM}^{\alpha_{CM}}\Gamma(\alpha_{CM}+1)}\right],\quad t\ll\tau_{CM}\left[2\frac{\Gamma(2\alpha_{CM})}{\Gamma(\alpha_{CM})}\right]^{1/\alpha_{CM}} \tag{11}$$

$$v_{Q_{CM}}(t)=IR_E\frac{t^{\alpha_{CM}}}{\tau_{CM}^{\alpha_{CM}}\Gamma(\alpha_{CM}+1)},\quad t\ll\tau_{CM}\left[2\frac{\Gamma(2\alpha_{CM})}{\Gamma(\alpha_{CM})}\right]^{1/\alpha_{CM}} \tag{12}$$

$$q_{Q_{CM}}(t)=I\frac{R_E}{R_E+R_I}t,\quad t\ll\tau_{CM}[\Gamma(\alpha_{CM}+2)]^{1/\alpha_{CM}} \tag{13}$$

If $R_E\gg R_I$, Eq. (13) can be written as

$$q_{Q_{CM}}(t)=It,\quad t\ll\tau_{CM}[\Gamma(\alpha_{CM}+2)]^{1/\alpha_{CM}},\quad R_E\gg R_I \tag{14}$$

Comparing the previous constraints, we see that the condition which leads to $v_{Q_{ET}}(t)$ and $i_{Q_{CM}}(t)$ exhibit a power-law behavior (t^α) –see Eqs. (11) and (12)– is slightly more restrictive than the one that ensures that almost all injected charge ($I\times t$) is transferred to the CPE_{CM} –see Eq. (13)–. It is clear that, in the limit α_{CM}=1, Eqs. (7), (8), and (10) show exponential relaxation patterns, and thus the two constraints provide the same result: $t\ll 2\tau_{CM}$. Furthermore, we should point out that the difference between these two "waiting times" increases as the values of α decrease. Thus, the condition of Eq. (13) can be successfully used when one assumes sufficiently short times of t and $\alpha\to1$ (the non-ideal capacitance of the system under study is close to the ideal case) [5]. Nevertheless, the selection of an optimal refinement condition to achieve an efficient coulostatic approach is satisfied through the constraint of Eqs. (11) or (12). For the reader's convenience, we have extracted this restriction and the final condition of Eq. (14), and now write them separately.

$$t\ll\tau_{CM}\left[2\frac{\Gamma(2\alpha_{CM})}{\Gamma(\alpha_{CM})}\right]^{1/\alpha_{CM}} \tag{15}$$

$$R_E\gg R_I \tag{16}$$

Fig. 2(b) and (c) show the waveform of $i_{Q_{CM}}(t)$ –see Eq. (7)– and, at sufficiently short times, a portion of the input current step and the graphical representation of Eq. (11), respectively. On the other hand, Fig. 2(d) shows the dynamic behavior of $v_{Q_{CM}}(t)$ of Eq. (8), which is similar to that of $i_{Q_{CM}}(t)$ of Eq. (7) –see Fig. 2(b)– but involves a Mittag-Leffler rise rather than a decay. The inset of Fig. 2(d) shows an expanded view corresponding to Eq. (12). For comparative purposes, the ideal exponential behavior (α_{CM}=1) is also set out in Fig. 2(b) and (d) –see dashed lines–. At short (long) times, it exhibits a slower (faster) decay than that of the Mittag-Leffler function.

2.2. Current step response of the electrode-tissue biointerface

The EEC of Fig. 1(b) can be analyzed from that of Fig. 1(c) by considering R_I=0 and renaming R_E, τ_{CM}, $i_{Q_{CM}}(t)$, $v_{Q_{CM}}(t)$, and $q_{Q_{CM}}(t)$ as R_P, τ_{ET}, $i_{Q_{ET}}(t)$, $v_{Q_{ET}}(t)$, and $q_{Q_{ET}}(t)$, respectively. τ_{ET} and $q_{Q_{ET}}(t)$ are the time constant for the EEC of Fig. 1(b) and the charge accumulated on CPE_{ET} (of parameters Q_{ET} and α_{ET}), respectively. Now, Eqs. (7)–(13) and (15) are rewritten as follows:

$$i_{Q_{ET}}(t)=IE_{\alpha_{ET}}\left[-\left(\frac{t}{\tau_{ET}}\right)^{\alpha_{ET}}\right],\quad t>0 \tag{17}$$

$$v_{Q_{ET}}(t)=IR_P\left(1-E_{\alpha_{ET}}\left[-\left(\frac{t}{\tau_{ET}}\right)^{\alpha_{ET}}\right]\right),\quad t>0 \tag{18}$$

$$\tau_{ET}=(R_PQ_{ET})^{1/\alpha_{ET}} \tag{19}$$

$$q_{Q_{ET}}(t)=ItE_{\alpha_{ET},2}\left[-\left(\frac{t}{\tau_{ET}}\right)^{\alpha_{ET}}\right],\quad t>0 \tag{20}$$

$$i_{Q_{ET}}(t)=I\left[1-\frac{t^{\alpha_{ET}}}{\tau_{ET}^{\alpha_{ET}}\Gamma(\alpha_{ET}+1)}\right],\quad t\ll\tau_{ET}\left[2\frac{\Gamma(2\alpha_{ET})}{\Gamma(\alpha_{ET})}\right]^{1/\alpha_{ET}} \tag{21}$$

$$v_{Q_{ET}}(t)=IR_P\frac{t^{\alpha_{ET}}}{\tau_{ET}^{\alpha_{ET}}\Gamma(\alpha_{ET}+1)},\quad t\ll\tau_{ET}\left[2\frac{\Gamma(2\alpha_{ET})}{\Gamma(\alpha_{ET})}\right]^{1/\alpha_{ET}} \tag{22}$$

$$q_{Q_{ET}}(t) = It, \quad t \ll \tau_{ET}[\Gamma(\alpha_{ET}+2)]^{1/\alpha_{ET}} \tag{23}$$

$$t \ll \tau_{ET}\left[2\frac{\Gamma(2\alpha_{ET})}{\Gamma(\alpha_{ET})}\right]^{1/\alpha_{ET}} \tag{24}$$

We also note that Eqs. (17)–(24) can be derived from a previous paper by the authors [5], which focused on a generalized procedure for the coulostatic method using a CPE. Finally, it should be mentioned that the corresponding exponential behaviors (ideal capacitances) can be found by setting α_{ET}=1 in Eqs. (17)–(24). Fig. 2(e), (c), (f), and the inset of Fig. 2(f) show the graphical representations of Eqs. (17), (21), (18), and (22), respectively. The dashed lines indicate $i_{Q_{ET}}(t)$ and $v_{Q_{ET}}(t)$ for the exponential behavior (α_{ET}=1).

2.3. Pulse- and impulse-response of the current-excited electrode-tissue system

From a theoretical point of view, two critical issues emerge on considering the fractional-order dispersive behavior of the bioelectrochemical system under study using the coulostatic technique: (i) an instantaneous change in the charge q_{in} (impulse) involves infinite (time-dependent) values of voltage and current for both CPEs, and (ii) the shape of the coulostatic pulse is of critical importance in the method (e.g., relaxation processes). Note that, in the ideal cases (α_{CM}=1 and α_{ET}=1), the charge injected during the application of the impulse causes the voltage to vary from 0 to $(q_{in}R_E)/[C_{CM}(R_E+R_I)]$ or q_{in}/C_{ET} (finite values) for the EECs of Fig. 1(c) or 1(b), respectively. Furthermore, the shape of the coulostatic pulse is unimportant [1,25].

To illustrate, we study the behavior of the EECs of Fig. 1(c) and (b) in response to the rectangular current pulses of width T and height I (Fig. 3(a)), commonly used in practice. For convenience, in Eq. (25), the pulses of current have been stated explicitly in terms of the charge q_{in} to be transferred and T.

$$I = \frac{q_{in}}{T}, \quad 0 < t < T \tag{25}$$

that is,

$$i(t) = \frac{q_{in}}{T}[u(t) - u(t-T)]$$

In effect, if $T\to 0$ and $(q_{in}/T)\to\infty$, the pulses approach an impulse function of strength q_{in} (refer to Fig. 3(a)). As long as $i_{Q_{CM}}(t)$ and $i_{Q_{ET}}(t)$ are roughly constant for $0<t<T$, it can be clearly seen that $v_{Q_{CM}}(T)$ and $v_{Q_{ET}}(T)$ are directly proportional to $T^{\alpha-1}$ (time-dependent characteristic). At time $t=T$, the negative step change of the pulse occurs and both voltage values tend to infinity when the pulse duration tends to zero (delta function),

$$v_{Q_{CM}}(T) = \frac{q_{in}}{Q_{CM}}\frac{R_E}{R_E+R_I}\frac{T^{\alpha_{CM}-1}}{\Gamma(\alpha_{CM}+1)} \to \infty, \quad T \to 0$$

$$v_{Q_{ET}}(T) = \frac{q_{in}}{Q_{ET}}\frac{T^{\alpha_{ET}-1}}{\Gamma(\alpha_{ET}+1)} \to \infty, \quad T \to 0$$

Note that these expressions can be found by substituting Eq. (25) in Eqs. (12) and (22) at $t=T$ and using Eqs. (9) and (19), respectively. This unexpected pattern can be explained from the electrical representation of a CPE, which involves equivalent networks built up from an infinite number of RC subcircuits [26]. Immediately after the current is switched off, a relaxation process occurs. Indeed, the coulostatic method can be interpreted from the perspective of a current interruption method (CIM) where the constant current is applied for a sufficiently short time (much lower than the time constant τ) [7,8]. Once on open circuit ($i(t)$=0 A), CPEs will be discharged through the local resistances (R_E+R_I and R_P in the EECs of Fig. 1(c) and (b), respectively) and thus, the "internal currents", $i_{R_{CM}}(t)$ and $i_{R_{ET}}(t)$, could be expressed as

$$i_{R_{CM}}(t) = -i_{Q_{CM}}(t) = -Q_{CM}\frac{d^{\alpha_{CM}}v_{Q_{CM}}(t)}{dt^{\alpha_{CM}}}$$

$$i_{R_{ET}}(t) = -i_{Q_{ET}}(t) = -Q_{ET}\frac{d^{\alpha_{ET}}v_{Q_{ET}}(t)}{dt^{\alpha_{ET}}}$$

where the corresponding voltages moves back toward 0 V, i.e., $v_{Q_{CM}}(t)$ and $v_{Q_{ET}}(t)$ decrease from $q_{in}R_ET^{\alpha-1}/[Q_{CM}(R_E+R_I)\Gamma(\alpha_{CM}+1)]$ or $q_{in}T^{\alpha-1}/[Q_{ET}\Gamma(\alpha_{ET}+1)]$ (CPE voltage cannot change abruptly) to 0 V, as [5]

$$v_{Q_{CM}}(t) = \frac{q_{in}}{Q_{CM}}\frac{R_E}{R_E+R_I}\frac{T^{\alpha_{CM}-1}}{\Gamma(\alpha_{CM}+1)}E_{\alpha_{CM}}\left[-\left(\frac{t-T}{\tau_{CM}}\right)^{\alpha_{CM}}\right], \quad t > T \tag{26}$$

$$v_{Q_{ET}}(t) = \frac{q_{in}}{Q_{ET}}\frac{T^{\alpha_{ET}-1}}{\Gamma(\alpha_{ET}+1)}E_{\alpha_{ET}}\left[-\left(\frac{t-T}{\tau_{ET}}\right)^{\alpha_{ET}}\right], \quad t > T \tag{27}$$

Eqs. (26) and (27) constitute the analytical expressions of the subsequent open-circuit discharges for the EECs shown in Fig. 1(c) and (b), respectively, when one approximates the charge impulse by a sufficiently short current pulse. In order to establish a comparison between a rectangular and a delta function type of pulse (input) –see Eqs. (25) and (2), respectively– in terms of coulostatic relaxation curves (output), we first obtain the impulse responses of $v_{Q_{CM}}(t)$ and $v_{Q_{ET}}(t)$:

$$v_{Q_{CM}}(t) = \frac{q_{in}}{Q_{CM}}\frac{R_E}{R_E+R_I}t^{\alpha_{CM}-1}E_{\alpha_{CM},\alpha_{CM}}\left[-\left(\frac{t}{\tau_{CM}}\right)^{\alpha_{CM}}\right]u(t) \tag{28}$$

$$v_{Q_{ET}}(t) = \frac{q_{in}}{Q_{ET}}t^{\alpha_{ET}-1}E_{\alpha_{ET},\alpha_{ET}}\left[-\left(\frac{t}{\tau_{ET}}\right)^{\alpha_{ET}}\right]u(t) \tag{29}$$

It can be clearly seen that both expressions show a prominent deviation from the pulse responses and thus, it allows us to confirm that, although the excitation exhibits a coulostatic nature, the type of excitation signal determines the shape of the relaxation curve in the context of non-ideal capacitive effects. Fig. 3(b) and (c) summarize the evolution of the coulostatic charging-discharging processes when T decreases and (q_{in}/T) increases: As $T\to 0$ and $(q_{in}/T)\to\infty$, the voltage responses $v_{Q_{CM}}(t)$ and $v_{Q_{ET}}(t)$ for $0<t<T$ become steeper and steeper, and finally, $v_{Q_{CM}}(T)\to\infty$ and $v_{Q_{ET}}(T)\to\infty$ (see above).

Analogously, Fig. 3(d) and (e) show the waveforms of $i_{Q_{CM}}(t)$ and $i_{Q_{ET}}(t)$, respectively. In effect, the resulting currents can be found as the product of Q_{CM} or Q_{ET} and the fractional-order derivative (d^α/dt^α, $0<\alpha<1$) of their respective voltages, $v_{Q_{CM}}(t)$ or $v_{Q_{ET}}(t)$. The portions of the initial-decay regions in pulse responses correspond to coulostatic charge injections (i.e., Eqs. (9), (11), (19), (21), and (25)). Note that our predictions make sense because the CPE voltage cannot change instantaneously and, thus, the step change, at time $t=T$, yields jump discontinuities (as those at t=0). In turn, these iR-drops involve infinite discontinuities when $T\to 0$, seen at the instant immediately following the step change ($t=T^+$):

$$i_{Q_{CM}}(T^+) = -q_{in}\frac{R_E}{R_E+R_I}\frac{T^{\alpha_{CM}-1}}{\tau_{CM}^{\alpha_{CM}}\Gamma(\alpha_{CM}+1)} \to -\infty, \quad T \to 0$$

$$i_{Q_{ET}}(T^+) = -q_{in}\frac{T^{\alpha_{ET}-1}}{\tau_{ET}^{\alpha_{ET}}\Gamma(\alpha_{ET}+1)} \to -\infty, \quad T \to 0$$

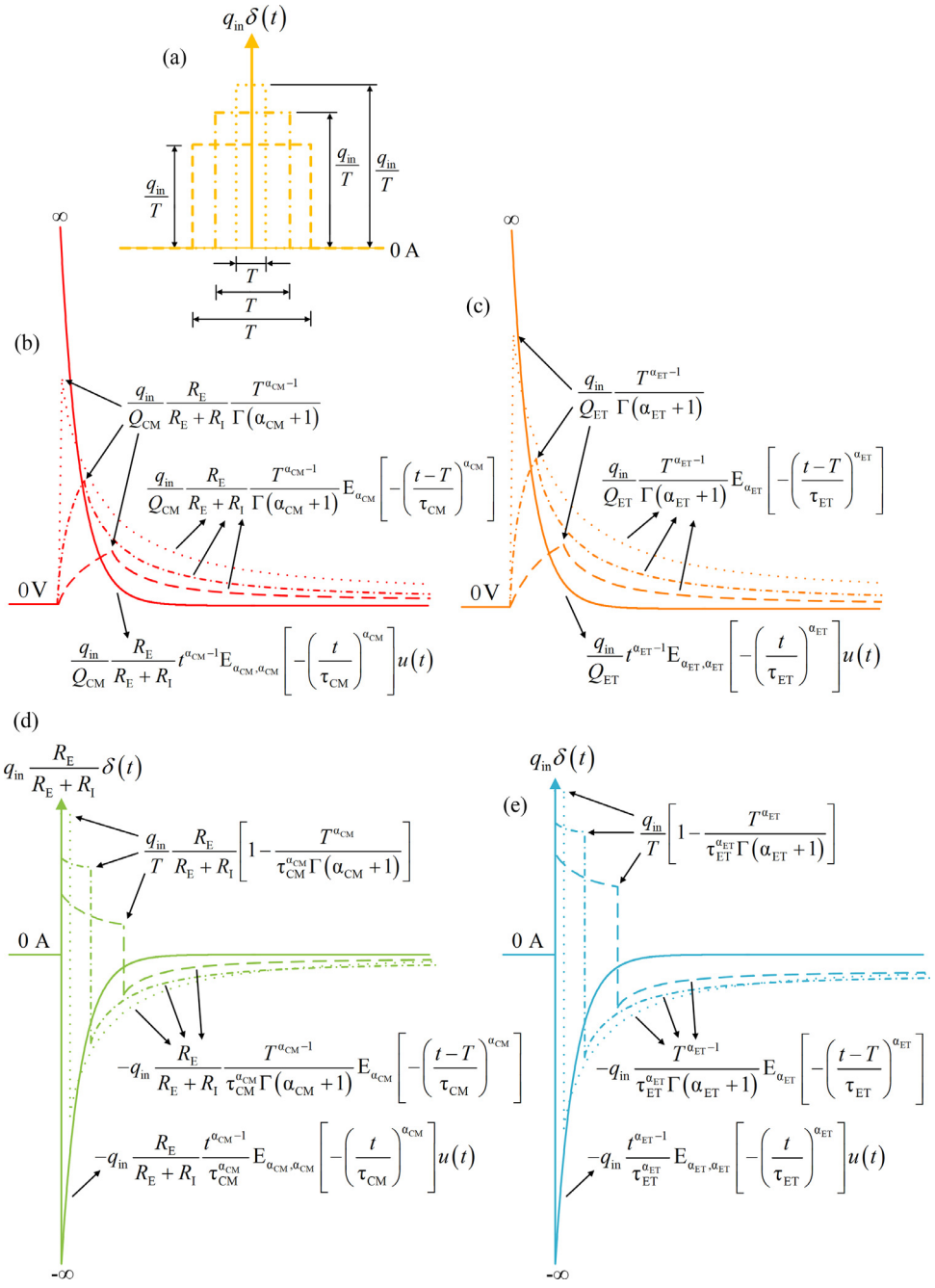

Fig. 3. Schematic of coulostatic relaxation processes depending on the shape of the signal excitation: (a) Sequence of $i(t)$ as $T\to 0$ and $(q_{in}/T)\to\infty$ (from a rectangular to a delta function type of pulse); (b) and (c), subsequent transient-voltage responses of CPE_{CM} and CPE_{ET}, respectively, i.e., $v_{Q_{CM}}(t)$ and $v_{Q_{ET}}(t)$, described in terms of Mittag-Leffler functions; (d) and (e), waveforms of the resulting non-ideal capacitive current of CPE_{CM} and CPE_{ET}, respectively, $i_{Q_{CM}}(t)$ and $i_{Q_{ET}}(t)$, in response to the excitation signals of (a).

For any value of time after charge injection ($t>T$), considering a sufficiently short duration rectangular current pulse as the excitation signal, both currents can be expressed as

$$i_{Q_{CM}}(t) = -q_{in}\frac{R_E}{R_E+R_I}\frac{T^{\alpha_{CM}-1}}{\tau_{CM}^{\alpha_{CM}}\Gamma(\alpha_{CM}+1)}E_{\alpha_{CM}}\left[-\left(\frac{t-T}{\tau_{CM}}\right)^{\alpha_{CM}}\right], \quad t>T \tag{30}$$

$$i_{Q_{ET}}(t) = -q_{in}\frac{T^{\alpha_{ET}-1}}{\tau_{ET}^{\alpha_{ET}}\Gamma(\alpha_{ET}+1)}E_{\alpha_{ET}}\left[-\left(\frac{t-T}{\tau_{ET}}\right)^{\alpha_{ET}}\right], \quad t>T \tag{31}$$

On the contrary, the current relaxation processes, in the case of a "pure coulostatic impulse (delta type)" input, can be expressed mathematically as follows:

$$i_{Q_{CM}}(t) = q_{in}\frac{R_E}{R_E+R_I}\delta(t) - q_{in}\frac{R_E}{R_E+R_I}\frac{t^{\alpha_{CM}-1}}{\tau_{CM}^{\alpha_{CM}}}E_{\alpha_{CM},\alpha_{CM}}\left[-\left(\frac{t}{\tau_{CM}}\right)^{\alpha_{CM}}\right]u(t) \tag{32}$$

$$i_{Q_{ET}}(t) = q_{in}\delta(t) - q_{in}\frac{t^{\alpha_{ET}-1}}{\tau_{ET}^{\alpha_{ET}}}E_{\alpha_{ET},\alpha_{ET}}\left[-\left(\frac{t}{\tau_{ET}}\right)^{\alpha_{ET}}\right]u(t) \tag{33}$$

In general, the theoretical background previously outlined enables us to determine that, immediately after the application of the current impulse, the shape of the resulting waveforms is similar to those for current-excited pulse responses (relaxation functions of the Mittag–Leffler type). Nevertheless, impulse responses show more complicated behaviors: In the limit (delta function), all the resulting waveforms suffer infinite discontinuities, and also involve faster decay rates than those of the pulse current input. Therefore, this straightforward procedure, which is a well-established methodology for ideal behaviors ($\alpha_{CM}=1$ and $\alpha_{ET}=1$), leads to a

significant problem in the context of the charge-step method considering non-ideal capacitive effects: The coulostatic decays are not described in terms of the same relaxation functions when the shape of the step-charge supplied to the system is different –one- or two-parameter Mittag-Leffler functions, see Eqs. (26)–(33). This should be taken into account in the "graphical analysis" process of experimental data in order to obtain accurate values of the electrical parameters and the underlying bioelectrochemical processes.

3. Discussion

Again, we begin with the analysis of the tissue response. Depending on the time scale considered, the value of (t/τ_{CM}) governs the non-exponential behavior of Fig. 2(b), which involves the decreasing expression of Eq. (11) at sufficiently short times, as shown in Fig. 2(c). Remember that the Mittag-Leffler function exhibits two asymptotic approximations: an initial fast decay described by the stretched exponential function (preceded earlier by Eq. (11)) and a long tail (inverse power-law behavior) [27–29]. We note that the areas under a portion of the waveforms of the current step of Fig. 2(a) and $i_{Q_{CM}}(t)$ of Fig. 2(b) are equal to the electrical charges injected, during that time interval, into the tissue (EEC of Fig. 1(c)) and cell membranes (modeled as a whole by CPE_{CM}), respectively. Specifically, Eq. (10) quantifies the electrical charge accumulated on CPE_{CM} during the interval $t = 0$ to t, but we are interested in sufficiently short times in which the tissue exhibits "electrical inertia" (i.e., $t \ll \tau_{CM}$).

At times satisfying the constraint imposed by Eq. (15), the area under the waveform of $i_{Q_{CM}}(t)$ is the charge transferred to the cell membranes. However, this area is rather lower than that of the portion of the input current step. The difference between the two areas involves dissipative losses in the extra- and intra-cellular media (R_E and R_I, respectively). Thus, the efficiency of a coulostatic charging process in a tissue is mainly limited via the extracellular path R_E. We then see that at sufficiently short times, given by Eq. (15), and if $R_E \gg R_I$ [18] (see Eq. (16)), the charge transferred to CPE_{CM} increases and closely approaches a coulostatic charge injection. In effect, Eq. (14) yields $I \times t$ which is the charge accumulated on CPE_{CM}, and, in turn, the charge injected into the tissue from the input current step, that is, a coulostatic charging process. As mentioned earlier, an ideal coulostatic charging injection is achieved as long as CPE_{CM} is replaced by a capacitor, the input current is an impulse and $R_E/(R_I+R_E)=1$ (i.e. $R_E \to \infty$ or $R_I=0$).

Apart from the notation, as indicated in the last section, Eqs. (17)–(24) are the same as Eqs. (7)–(13) and (15) when R_I is set to zero. Therefore, the waveforms of $i_{Q_{ET}}(t)$ and $v_{Q_{ET}}(t)$ present similar non-exponential dynamics (regarding the electrode-tissue interface) to those of $i_{Q_{CM}}(t)$ and $v_{Q_{CM}}(t)$, respectively. Finally, it is important to note that an effective coulostatic charging process of the electrode-tissue interface is achieved at times satisfying the constraint of Eq. (24).

Let us return to the EEC of the electrode-tissue-electrode system (refer to Fig. 1). The interconnection of the EECs of Fig. 1(b) and (c) provides a modified Randles circuit [5], by replacing the series resistance by the modified Fricke and Morse EEC [7]. This expanded circuit allows the anomalous capacitive behavior of both phenomena (biointerfacial and tissue processes) to be captured effectively in a simple manner. From an experimental point of view, the study of this double-dispersion model (with different orders of the fractional derivative, $\alpha_{CM} \neq \alpha_{ET}$) involves a more realistic analysis than the classical one. It supposes a generalized procedure that leads to an in-depth understanding of the underlying bioelectrochemical and physiological processes (taking into account non-local interactions and system memory effects). Nevertheless, our model introduces the inherent difficulty of the fractional derivative: This is clearly evident if there is a substantial overlap between the two cooperative relaxation phenomena (distribution of time constants), that is, τ_{CM} comparable to τ_{ET}. We note that values of the order of μs and s for τ_{CM} and τ_{ET}, respectively, were previously obtained by the authors: $\tau_{CM} \ll \tau_{ET}$ [5,7,8]. Thus, the constraint of Eq. (24) may appear more limiting than that of Eq. (15). In this sense, the coulostatic method, along with a two-electrode measuring system, could be successfully implemented to obtain the electrical properties of biological tissues. This experimental protocol could provide immunity to the influence of the electrode polarization impedance if $\tau_{ET} \gg \tau_{CM}$, while maintaining the intrinsic advantages of the method and the measuring setup. In any case, a four-electrode arrangement could be used to avoid the effects of the electrode polarization.

The discussion above enables us to draw the following conclusions for an electrode-tissue-electrode system driven by a current step input: (i) The constraints of Eqs. (15) –sufficiently short times– and (16) –limitation imposed by the extra-cellular resistance– must be satisfied for an efficient coulostatic charging process in the tissue; (ii) the constraint of Eq. (24) at sufficiently short times must be satisfied for an efficient coulostatic charge injection into the electrode/tissue interface; and (iii) the constraints of Eqs. (15), (16), and (24) must be satisfied at the same time to guarantee an efficient coulostatic charging process in the electrode-tissue-electrode system. During the charge injection, CPEs thus act as short circuits (all the current flows through the cell membranes and non-ideal biointerfacial capacitance) and no current flows through: (i) R_E –the membrane effects disappear: the current flows everywhere according to local ionic conductivity–; and (ii) R_P –the faradaic reactions can be neglected–. Indeed, an appropriate selection of the pulse duration is important to charge only the non-ideal capacitances, and to avoid faradaic processes and extra-cellular interactions which would occur at higher levels of total charge with longer pulses. Our model considers the perturbation time required to perform an efficient coulostatic approach applied to an electrode-tissue-electrode system, taking into account its complex and multiscale dynamics (anomalous evolution of transient responses). This is a very serious issue, because erroneous duration pulses, apart from being time-consuming, could also possibly inject toxic materials into the tissue, cause pH changes in the portion of the tissue immediately adjacent to the electrode surface, or induce thermal injuries, via faradaic processes. Furthermore, this would result in bad estimates for the electrical properties of the system through the coulostatic relaxation processes. Thus, fractional calculus plays a crucial role to obtain accurate information about the electrical properties of many "real-world systems", in particular, the tissue-electrode processes, using the coulostatic method.

As a final remark, it should be mentioned that the shape of the pulse is of fundamental importance in the method, although the coulostatic nature and the strength of the pulse (q_{in}) are retained. The essential differences consist of the transient dynamics in which: (i) the step-charge is transferred to the CPEs and, even more importantly, (ii) the distributed relaxation processes move back towards the equilibrium state. For instance, the impulse responses involve infinite discontinuities and faster relaxation phases than those of the pulse responses (see Fig. 3(b)–(e) and Eqs. (26)–(33)) and should therefore be taken into account when one determines the parameter values of the EECs under study. In comparison with ideal capacitive behavior (classical view), the discharge process of a CPE (cell membranes at the tissue level and the electrode biointerfacial regions) depends on the type of charging waveform. Thus, our results can be used to pave the way to finding more adapted excitation waveforms to estimate the electrical properties of these types of bielectrochemical systems in the context of the coulostatic method.

4. Conclusions

In an electrode-tissue-electrode system driven by a constant dc current, we have established the required constraints at sufficiently short times for an effective coulostatic charge injection, capturing the fractional-order dispersive behavior (CPE) of the interfaces and the biological material. In this sense, it is demonstrated that the coulostatic charging process in a tissue is limited via the extracellular path. Also, we show how the shape of the excitation signal (e.g., a rectangular or a delta function type of pulse) affects the transient dynamics of the coulostatic relaxation processes, using the mathematical tools of fractional calculus. This methodology can be extended to include coulostatic charging of membranes of organelles, at the tissue or cellular level. Furthermore, a coulostatic test method could be implemented to characterize the electrical properties of the electrode-tissue-electrode, or even the electrical properties of the tissue itself, if the contribution of the electrode-tissue interface can be neglected (i.e., $\tau_{ET} \gg \tau_{CM}$). In any case, a four-electrode arrangement could be used to avoid the effects of electrode polarization. We hope that the reader will find this methodology useful, with possibilities of implementation in the context of a very wide range of bio-applications.

Credit author statement

All work in this single-author paper has been carried out by Enrique Hernández-Balaguera.

Declaration of Competing Interest

The authors declare that they have no known competing financial interests or personal relationships that could have appeared to influence the work reported in this paper.

Acknowledgements

This work has been supported by the Comunidad de Madrid under the SINFOTON2-CM Research Program, S2018/NMT4326-SINFOTON2-CM, the Ministerio de Economía, Industria y Competitividad, Projects MTM2016–80539-C2–1-R and TEC2016–77242-C3–3-R, the Consejería de Educación, Cultura y Deportes of the Junta de Comunidades de Castilla-La Mancha, Project SBPLY/17/180501/000380, and the European Regional Development Fund (fondos FEDER).

References

[1] van Leeuwen HP. The coulostatic impulse technique: A critical review of its features and possibilities. Electrochim Acta 1978;23:207–18.
[2] Delahay P. Coulostatic method for kinetic study of fast electrode processes. I. Theory. J Phys Chem 1962;66:2204–7.
[3] Reinmuth WH. Theory of coulostatic impulse relaxation. Anal Chem 1962;34:1272–6.
[4] Kanno K, Suzuki M, Sato Y. An application of coulostatic method for rapid evaluation of metal corrosion rate in solution. J Electrochem Soc 1978;125:1389–93.
[5] Hernández-Balaguera E, Polo JL. A generalized procedure for the coulostatic method using a constant phase element. Electrochim Acta 2017;233:167–72.
[6] Merrill DR, Bikson M, Jefferys JGR. Electrical stimulation of excitable tissue: design of efficacious and safe protocols. J Neurosci Methods 2005;141:171–98.
[7] Hernández-Balaguera E, López-Dolado E, Polo JL. Obtaining electrical equivalent circuits of biological tissues using the current interruption method, circuit theory and fractional calculus. RSC Adv. 2016;6:22312–19.
[8] Hernández-Balaguera E, López-Dolado E, Polo JL. *In vivo* rat spinal cord and striated muscle monitoring using the current interruption method and bioimpedance measurements. J Electrochem Soc 2018;165(12):G3099–103.
[9] Westerlund S, Ekstam L. Capacitor theory. In: IEEE T on Dielect El, 1; 1994. p. 826–39.
[10] Xu J, Mi CC, Cao B, Cao J. A new method to estimate the state of charge of lithium-ion batteries based on the battery impedance model. J Power Sources 2013;233:277–84.
[11] Wang B, Li SE, Peng H, Liu Z. Fractional-order modeling and parameter identification for lithium-ion batteries. J Power Sources 2015;293:151–61.
[12] Hidalgo-Reyes JI, Gómez-Aguilar JF, Escobar-Jiménez RF, Alvarado–Martínez VM, López-López MG. Classical and fractional-order modeling of equivalent electrical circuits for supercapacitors and batteries, energy management strategies for hybrid systems and methods for the state of charge estimation: A state of the art review. Microelectron J 2019;85:109–28.
[13] Allagui A, Freeborn TJ, Elwakil AS, Fouda ME, Maundy BJ, Radwan AG, Said Z, Abdelkareem MA. Review of fractional-order electrical characterization of supercapacitors. J Power Sources 2018;400:457–67.
[14] Bisquert J. Theory of the impedance of electron diffusion and recombination in a thin layer. J Phys Chem B 2002;106:325–33.
[15] Zhang D, Allagui A, Elwakil AS, Nassef AM, Rezk H, Cheng J, Choy WCH. On the modeling of dispersive transient photocurrent response of organic solar cells. Org Electron 2019;70:42–7.
[16] Hernández-Balaguera E, Romero B, Arredondo B, del Pozo G, Najafi M, Galagan Y. The dominant role of memory-based capacitive hysteretic currents in operation of photovoltaic perovskites. Nano Energy 2020;78:105398.
[17] Sun H, Zhang Y, Baleanu D, Chen W, Chen Y. A new collection of real world applications of fractional calculus in science and engineering. Commun Nonlinear Sci Numer Simulat 2018;64:213–31.
[18] Brown DW, Bahrami AJ, Canton DA, Mukhopadhyay A, Campbell JS, Pierce RH, Connolly RJ. Development of an adaptive electroporation system for intratumoral plasmid DNA delivery. Bioelectrochemistry 2018;122:191–8.
[19] Hernández-Labrado GR, Polo JL, López-Dolado E, Collazos-Castro JE. Spinal cord direct current stimulation: finite element analysis of the electric field and current density. Med Biol Eng Comput 2011;49:417–29.
[20] Schoenbach KH, Katsuki S, Stark RH, Buescher ES, Beebe SJ. Bioelectrics-new applications for pulsed power technology. IEEE T Plasma Sci 2002;30:293–300.
[21] Yao C, Hu X, Mi Y, Li C, Sun C. Window effect of pulsed electric field on biological cells. IEEE T Dielect El In 2009;16:1259–66.
[22] Podlubny I. Fractional differential equations: An introduction to fractional derivatives, fractional differential equations, to methods of their solution and some of their applications. Academic Press; 1999.
[23] Magin RL. Fractional calculus in bioengineering, Part 1. Crit Rev Biomed Eng 2004;32:1–104.
[24] Reller H, Kirowa-Eisner E. The coulostatic method with finite pulse width. J Electrochem Soc 1987;134:126–32.
[25] Bard AJ, Faulkner LR. Electrochemical methods: fundamentals and applications. John Wiley & Sons; 2001.
[26] Hirschorn B, Orazem ME, Tribollet B, Vivier V, Frateur I, Musiani M. Determination of effective capacitance and film thickness from constant-phase element parameters. Electrochim Acta 2010;55:6218–27.
[27] Hernández-Balaguera E, Vara H, Polo JL. Identification of capacitance distribution in neuronal membranes from a fractional-order electrical circuit and whole-cell patch-clamped cells. J Electrochem Soc 2018;165(12):G3104–11.
[28] Mainardi F. On some properties of the Mittag-Leffler function $E\alpha(-t\alpha)$, completely monotone for t>0 with $0<\alpha<1$. Discrete Contin Dyn Syst Ser B 2014;19:2267–78.
[29] Hernández-Balaguera E, Polo JL. On the potential-step hold time when the transient-current response exhibits a Mittag-Leffler decay. J Electroanal Chem 2020;856:113631.